Chinese Chemical Letters 35 (2024) 108561

Contents lists available at ScienceDirect

Chinese Chemical Letters

journal homepage: www.elsevier.com/locate/cclet

Enabling superior electrochemical performance of NCA cathode in $Li_{5.5}PS_{4.5}Cl_{1.5}$-based solid-state batteries with a dual-electrolyte layer

Ziling Jiang[a,b], Shaoqing Chen[c], Chaochao Wei[a], Ziqi Zhang[b], Zhongkai Wu[a], Qiyue Luo[a], Liang Ming[a], Long Zhang[d,*], Chuang Yu[a,b,*]

[a] School of Chemistry and Chemical Engineering, Huazhong University of Science and Technology, Wuhan 430074, China
[b] State Key Laboratory of Advanced Electromagnetic Engineering and Technology, School of Electrical and Electronic Engineering, Huazhong University of Science and Technology, Wuhan 430074, China
[c] Innovation Center for Chemical Sciences, College of Chemistry, Chemical Engineering and Materials Science, Soochow University, Suzhou 215123, China
[d] College of Physics and Energy, Fujian Normal University, Fuzhou 350117 China

ARTICLE INFO

Article history:
Received 17 March 2023
Revised 12 April 2023
Accepted 10 May 2023
Available online 13 May 2023

Keywords:
$LiNi_{0.8}Co_{0.15}Al_{0.05}O_2$
$Li_{5.5}PS_{4.5}Cl_{1.5}$
Double solid electrolyte layer configuration
Operating temperatures
Electrochemical performances

ABSTRACT

$LiNi_{0.8}Co_{0.15}Al_{0.05}O_2$ (NCA) is a promising cathode for sulfide-based solid-state lithium batteries (ASSLBs) profiting from its high specific capacity and voltage plateau, which yielding high energy density. However, the inferior interfacial stability between the bare NCA and sulfides limits its electrochemical performance. Hereien, the dual-electrolyte layer is proposed to mitigate this effect and enhance the battery performances of NCA-based ASSLIBs. The Li_3InCl_6 wih high conductivity and excellent electrochemcial stability act both as an ion additives to promote Li-ion diffusion across the interface in the cathode and as a buffer layer between the cathode layer and the solid electrolyte layer to avoid side reactions and improve the interface stability. The corresponding battery exhibits high discharge capacities and superior cyclabilities at both room and elevated temperatures. It exhibits discharge performance of 237.04 and 216.07 mAh/g at 0.1 and 0.5 C, respectively, when cycled at 60 °C, and sustains 95.9% of the capacity after 100 cycles at 0.5 C. The work demonstrates a simple strategy to ensure the superior performances of NCA in sulfide-based ASSLBs.

The electrification of transportation and large-scale energy storage has led to increased demands for lithium-ion batteries with improved safety, energy density, and cycle life [1,2]. However, traditional lithium-ion batteries using organic electrolytes present safety concerns and have nearly reached their energy density limits [3,4]. Solid-state batteries, which offer higher safety and energy density, are expected to fundamentally address these issues [5–9]. The electrochemical performance of ASSLB is bound up with the solid electrolyte, electrode, and interface properties between them. Among the developed solid electrolytes, sulfide electrolytes have good prospects as solid electrolyte candidates due to their high lithium ion conductivity, low interfacial resistance, and low Young's modulus [10,11]. In particular, our previous work found that halogen-enriched argyrodite solid electrolytes have high ion conductivity, which is comparable to the conductivity of current liquid electrolytes (10^{-2} S/cm) [12–14]. $LiNi_{0.8}Co_{0.15}Al_{0.05}O_2$ (NCA) has the advantages of high reversible capacity, low cost, low toxicity, and is considered one of the most promising lithium-ion battery cathode materials [15,16]. However, the interface instability between oxide cathodes and sulfide electrolytes has long been a frustrating problem, resulting in poor rate and cycling performance of oxide cathodes, especially for Ni-rich layered oxide $LiNi_xCo_yMn/Al_{1-x-y}O_2$ ($x \geq 0.8$) [17].

Considerable efforts have been made to ameliorate the interface stability between oxide cathodes and sulfide electrolytes. A widely adopted and effective approach is to modify the surface of oxide cathode materials by coating them with a stable oxide layer, referred to as the buffer layer. This thin layer acts as a barrier between the oxide cathode and the sulfide electrolyte particles, preventing undesirable interfacial reactions. Lithium-containing buffer layers, such as $LiNbO_3$ [15,18-20], $Li_4Ti_5O_{12}$ [21,22], Li_2ZrO_3 [23,24] and Li_2SiO_3 [25,26], have been extensively used to stabilize the interface and reduce interfacial resistance for their superior interfacial lithium ion diffusion, lower resistance, and negligible capacity contribution. However, the choice of coating material, thickness, and shape can significantly affect battery performance. The coating of the buffer layer typically involves complex techniques such as

* Corresponding authors.
E-mail addresses: longzhang2023@163.com (L. Zhang), cyu2020@hust.edu.cn (C. Yu).

https://doi.org/10.1016/j.cclet.2023.108561
1001-8417/

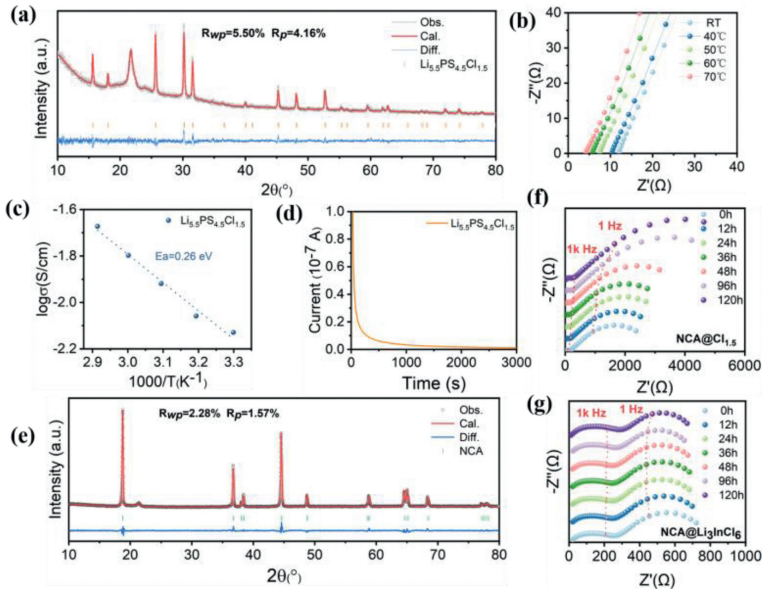

Fig. 1. (a) XRD refinement of the $Li_{5.5}PS_{4.5}Cl_{1.5}$ electrolyte. (b) The impedance spectra and (c) the corresponding Arrhenius plots of $Li_{5.5}PS_{4.5}Cl_{1.5}$ based on ionic conductivities measured at different temperatures. (d) The DC polarization plots of the $Li_{5.5}PS_{4.5}Cl_{1.5}$. (e) XRD refinement of the NCA cathode. (f) The changes in resistance over time of the cathode mixture consisting of NCA@$Cl_{1.5}$ and (g) NCA@Li_3InCl_6. Stainless steel (ST) was used as the blocking electrode during the measurement process.

electrochemical deposition, magnetron sputtering, and ALD/MLD, which require specialized equipment and high costs. Our previous works have demonstrated the (electro)chemical stability of Li_3InCl_6 with bare $LiNi_{0.6}Mn_{0.2}Co_{0.2}O_2$ [27]. The all-solid-state battery with Li_3inCl_6 isolation layer between $LiNi_{0.6}Mn_{0.2}Co_{0.2}O_2$ active material and sulfide electrolyte showed excellent electrochemical performance. However, the compatibility of Li_3InCl_6 with high-capacity Ni-rich layered oxide $LiNi_xCo_yMn/Al_{1-x-y}O_2$ ($x \geq 0.8$) has been little investigated, so we introduced Li_3InCl_6 between NCA and $Li_{5.5}PS_{4.5}Cl_{1.5}$.

In this study, we added the pure Li_3InCl_6 electrolytes both in the cathode mixture and as a separate layer between the cathode layer and solid electrolyte layer to isolate the direct contact between the bare NCA and $Li_{5.5}PS_{4.5}Cl_{1.5}$ electrolytes. Li_3InCl_6 acts as an ion additives to promote Li-ion conductivity and avoid the space charge effect in the cathode mixture. Moreover, the introduced layer can ensure the totally isolation between these two materials. The electrochemcial performances of ASSLBs with and without this dual-electrolyte layer are also investigated and compared at various charge/discharge current densities under different operating temperatures. The battery with dual-electrolyte layer configuration exhibits superior electrochemical performances at different test conditions. Multiple *ex-situ* characterization methods, such as XRD, SEM, TEM and XPS are combined to unuravel the working mechanism for this improvements.

The Cl-rich $Li_{5.5}PS_{4.5}Cl_{1.5}$ were chosen as solid electrolytes to investigate the all-solid-state battery performance of NCA cathode due to its ultrafast Li-ion conductivity compared to other sulfides as reported in our previous research [19]. It was synthesized with the typical mechanicalchemical route, which consisting of a high rotation speed milling process followed by a sintering treatment [28,29]. The chosen NCA cathode and the $Li_{5.5}PS_{4.5}Cl_{1.5}$ were measured with powder XRD and refined using the Rietveld method. All the reflections are indexed well to the argyrodite Li_7PS_6 structure with excellent refinement, indicating that the pure target argyrodite-structure $Li_{5.5}PS_{4.5}Cl_{1.5}$ electrolyte has been successfully synthesized in this work (Fig. 1a). Detailed refinement parameters are list in Table S1 (Supporting information). The existence of anion disorder in the structure predicts a high ionic conductivity [30]. The AC impedance results show that the total resistance of the stainless steel/$Li_{5.5}PS_{4.5}Cl_{1.5}$/stainless steel decrease with increasing operating temperatures, indicating the prepared material is a typical inorganic ion conductor. The Li-ion conductivy of 7.43 mS/cm is deduced from the room temperature resistance result for the obtained $Li_{5.5}PS_{4.5}Cl_{1.5}$ electrolyte (Fig. 1b). Based on the Arrhenius behavior, the temperature-dependent Li-ion conductivities yields a low activation energy of 0.26 eV (Fig. 1c). Moreover, the electronic conductivity of $Li_{5.5}PS_{4.5}Cl_{1.5}$ was measured using the DC polarization method. It demonstrates an extremely low electronic conductivity (2.1×10^{-9} S/cm). The prepared $Li_{5.5}PS_{4.5}Cl_{1.5}$ with high ionic conductivity and ultra low electronic conductivity suggests excellent characteristics as solid electrolyte for ASSLBs.

The NCA materials with high voltage plateau and large charge/discharge capacities possess great potential as cathode for lithium batteries to achieve high energy density. In Fig. 1e, the diffraction peaks of the NCA used in this work are well indexed with the layered structure. The space group is R-3m [31–33]. The detailed XRD refinement parameters of the NCA are shown in Table S2 (Supporting information). The corresponding lattice constants *a* and *c* are 2.86586 Å and 14.18720 Å, respectively, and the Li/Ni disorder in the structure is only 0.06%. This low cation disorder indicates that this NCA is a super layered cathode for lithium batteries [34]. Previous research has shown that sulfide solid electrolytes exhibit poor stability with transiation metal-containing layered structure cathode materials [35]. To investigate the chemical stability between the bare NCA and $Li_{5.5}PS_{4.5}Cl_{1.5}$ electrolyte, the evolution of resistance as a function of the storage durations for the assembled ST/NCA-$Li_{5.5}PS_{4.5}Cl_{1.5}$/ST cell are performed. As shown in Fig. 1f, this cell exhibits large resistance during the whole test process, especially for the NCA and $Li_{5.5}PS_{4.5}Cl_{1.5}$ electrolytes interfacial section. Moreover, a clear increase of the interfacial resistance is observed with increasing storage durations, suggesting the intrinsically chemical instability between those two materials. To mitigate the side reaction, Li_3InCl_6 electrolyte with high chemical/electrochemcial stability with layered cathode materials was synthesized and chosen to replace the $Li_{5.5}PS_{4.5}Cl_{1.5}$ electrolyte in the mixture. The XRD patterns and detailed refinement parameters of the Li_3InCl_6 are shown in Fig. S1 and Table S3 (Supporting information). In contrast, much smaller total resistance is detected for the new ST/NCA-Li_3InCl_6/ST cell and minor variations of the

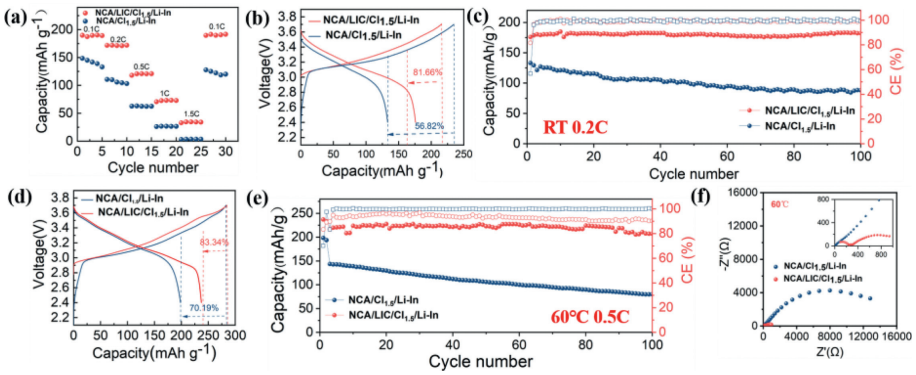

Fig. 2. Electrochemical performances of the assembled NCA/$Cl_{1.5}$/Li-In, and NCA/LIC/$Cl_{1.5}$/Li-In all-solid-state batteries. (a) The rate capability test result comparison of the above solid-state batteries. (b) The initial charge/discharge curves and (c) the corresponding cycling performances of the above batteries cycled at 0.2 C at room temperature. (d) The initial charge/discharge curves and (e) the corresponding cycling performances of the above batteries cycled at 0.5 C at 60 °C. (f) The impedance spectra of the above solid-state batteries after 100 cycles at 0.5 C at 60 °C.

resistance values are observed during the storage test in Fig. 1g, indicating that the prepared Li_3InCl_6 electrolyte displays excellent chemical stability with the bare NCA cathde. This implies that the it can act as solid electrolytes in the composite cathode for NCA-based ALLSBs.

To evoluate the charge-discharge performance, two kinds of battery configurations of $LiNi_{0.8}Co_{0.15}Al_{0.05}O_2$/$Li_{5.5}PS_{4.5}Cl_{1.5}$/Li-In (NCA/$Cl_{1.5}$/Li-In) and $LiNi_{0.8}Co_{0.15}Al_{0.05}O_2$-$Li_3InCl_6$/$Li_3InCl_6$/$Li_{5.5}PS_{4.5}Cl_{1.5}$/Li-In (NCA/LIC/$Cl_{1.5}$/Li-In) were constructed. Firstly, rate capability of the above two configuration batteries were investigated at RT. As shown in Fig. 2a, the NCA/$Cl_{1.5}$/Li-In battery shows poor discharge performances at various C-rates. Specifically, it delivers discharge capacities of 148.5 mAh/g at 0.1 C, 110.7 mAh/g at 0.2 C, 62.8 mA/g at 0.5C, 26.1 mAh/g at 1 C and 3.2 mAh/g at 1.5 C, respectively, and shows a discharge capacity value of 127.8 mAh/g when the rate recovers to 0.1 C. Due to the interfacial instability between bare NCA and the $Li_{5.5}PS_{4.5}Cl_{1.5}$, this battery displays low discharge capacities and even does not work at high C-rate, which agrees well with the published papers using sulfide electrolytes and bare NCA cathode [36–38]. In comparsion, the NCA/LIC/$Cl_{1.5}$/Li-In battery demonstrates better discharge performance than that of the NCA/$Cl_{1.5}$/Li-In battery at these C-rates under the same test conditions. It presents discharge capacities of 189.8, 171.7, 120.6, 72.7 and 34.4 mAh/g at 0.1, 0.2, 0.5, 1.0 and 1.5 C, respectively, and then recovers to 189.6 mAh/g when the C-rate lowers to 0.1 C. Further long-term cycling performances at different C-rates were also investigated. Both batteries were first cycled at 0.2 C between 3.0 V and 4.3 V (*vs.* Li^+/Li^0) under RT. As exhibited in Fig. 2b, the NCA/$Cl_{1.5}$/Li-In cell displays slowly increase of voltage since the beginning till 3.0 V (*vs.* Li-In), suggesting severe space charge effect occurs between bare NCA and $Li_{5.5}PS_{4.5}Cl_{1.5}$ in the composite cathode. Relatively speaking, the charge voltage of the NCA/LIC/$Cl_{1.5}$/Li-In battery reaches the same voltage directly, indicating that the Li_3InCl_6 electrolyte can mitigate the space charge effect between bare NCA and $Li_{5.5}PS_{4.5}Cl_{1.5}$ [35,39]. During the following initial discharge process, the former battery displays much lower discharge voltage plateau, while the latter batter with Li_3InCl_6 electrolyte exhibits higher discharge voltage plateau. The lowered discharge voltage plateau implies the loss of active Ni^{2+} in the cathode due to the side reaction between bare NCA and sulfide. For the cycling performance in Fig. 2c, the NCA/$Cl_{1.5}$/Li-In battery deliver an initial discharge capacity of 133.2 mAh/g at 0.2 C with a coulombic efficiency of 56.8%, and maintains a discharge capacity of 88.0 mAh/g with a capacity retention of 66.1% after 100 cycles. The low discharge capacities and poor cyclability are associated with the large interfacial resistances caused by the side reactions and space charge effect between bare NCA and $Li_{5.5}PS_{4.5}Cl_{1.5}$ [17]. In comparison, the NCA/LIC/$Cl_{1.5}$/Li-In battery delivers much higher discharge capacity of 175.9 mAh/g and coulombic efficiency of 81.7%, and sustains excellent cyclability with minor discharge capacity variations after 100 cycles (Fig. 2c). When the charge/discharge C-rate rises to 0.5 C, the NCA/$Cl_{1.5}$/Li-In battery demonstrates similar charge/discharge curves during the 1st cycle in Fig. S2a (Supporting information). It delivers a discharge capacity of 64.7 mAh/g at 0.5 C and only maintains a discharge capapcity of 40.2 mAh/g after 98 cycles. In contrast, the NCA/LIC/$Cl_{1.5}$/Li-In battery shows a discharge capacity of 104.3 mAh/g and retains 92.2% of this value after 98 cycles. The bare NCA with Li_3InCl_6 electrolyte exhibits much higher discharge capacities and superior cyclability at both 0.2 C and 0.5 C (Fig. S2c in Supporting information).

Furthermore, the battery performances at elevated temperature (60 °C) was also investigated. As demonstrated in Fig. 2d, the NCA/$Cl_{1.5}$/Li-In battery also suffers side reactions and space charge effect at 60 °C when cycled at 0.5 C based on the corresponding charge/discharge curves, while the Li_3InCl_6 in the NCA/LIC/$Cl_{1.5}$/Li-In battery can effective avoid these influences. At a higher operating temperature, both batteries exhibit much higher initial discharge capacity and coulombic efficiency than that at room temperature due to the activation of NCA cathode in the battery. During the first two cycles at 0.1 C, the former battery delivers a discharge capacity of 200.0 mAh/g for the 1st cycle, while the latter battery with Li_3InCl_6 electrolyte shows a higher discharge capacity of 237.04 mAh/g. For the subsequent cycling test at 0.5 C, discharge capacities of the NCA/$Cl_{1.5}$/Li-In battery decaies rapidly with a capacity retention of 34.75% after 98 cycles, while the other NCA/LIC/$Cl_{1.5}$/Li-In battery shows a strating discharge capacity of 216.1 mAh/g and sustains a discharge capacity of 207.27 mAh/g with a much higher capacity retention of 95.92% (Fig. 2e). Table S4 (Supporting information) compares the battery properties with the other representative sulfide-based solid-state lithium batteries of NSCA cathode. The battery in this work exhibits superior electrochemical performance. After 98 cycles at 0.5 C, the NCA/LIC/$Cl_{1.5}$/Li-In battery displays a much smaller resistance than that of the NCA/$Cl_{1.5}$/Li-In battery (over 12,000 Ω) in Fig. 2f, which vertifies our above analysis. The total resistance of NCA/$Cl_{1.5}$/Li-In battery after 98 cycles at 60 °C is almost 10 times higher than that at room temperature, suggesting that the elevated operating temperature accelerate side reactions between bare NCA and $Li_{5.5}PS_{4.5}Cl_{1.5}$, which in turn largrly increase the resistance for the battery during cycling, leading to a sharp deterioration of discharge

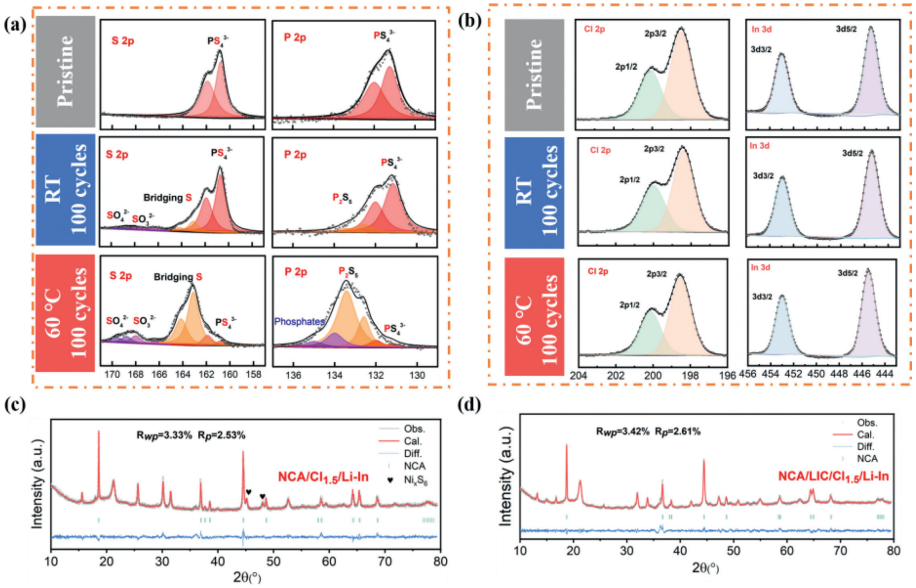

Fig. 3. XPS spectra of the cathode mixture before and after cycling for (a) the assembled NCA/$Cl_{1.5}$/Li-In and (b) NCA/LIC/$Cl_{1.5}$/Li-In solid-state lithium batteries at 0.5 C at different temperature. The XRD refinements of the cycled cathode mixture for (c) the assembled NCA/$Cl_{1.5}$/Li-In and (d) NCA/LIC/$Cl_{1.5}$/Li-In solid-state lithium batteries at 0.5 C at 60 °C.

capacities in Fig. 2e. While for the NCA/LIC/$Cl_{1.5}$/Li-In battery, it shows much smaller total battery resistances under both temperatures. Additionally, it demonstrates smaller resistance at 60 °C than that at room temperature (848.4 Ω *vs.* 922.5 Ω). During long cycles at both temperatures, the Li_3InCl_6 electrolyte in the configuration act both as Li-ions conducting additive in the composite cathode and as isolation layer between the NCA and $Li_{5.5}PS_{4.5}Cl_{1.5}$, resulting in superior electrochemcial performances. The faster Li-ion mobilities of different Li-containg materials at elevated temperature in the battery configuration including the solid electrolytes and active materials also provide higher capacities. On the other hand, the inherent incompatibility between $Li_{5.5}PS_{4.5}Cl_{1.5}$ and pristine NCA in the cathode is also accelerated, yielding fast capacity loss and intense electrochemical polarizations at higher temperatures.

The d*Q*/d*V* curves of those chosen cycles (1st, 25th, 50th, 75th and 100th) for the NCA/$Cl_{1.5}$/Li-In and NCA/LIC/$Cl_{1.5}$/Li-In batteries at 0.5 C at 60 °C were also performed to further unravel the structural variations. The d*Q*/d*V* curves reflect the characteristic redox peaks associated with the multiple phase transitions that occuring during the lithiation and delithiation processes. As shown in Fig. S3 (Supporting information), both the assembled NCA/$Cl_{1.5}$/Li-In and NCA/LIC/$Cl_{1.5}$/Li-In batteries show four distinct oxidation peaks in the first cycle, indicating that all cathodes undergo a series of phase transitions (H1-M-H2-H3) [40]. During 100 cycles, the voltage difference between the oxidation/reduction d*Q*/d*V* peaks increases with increasing cycle number for the NCA/$Cl_{1.5}$/Li-In battery. Additionally, in subsequent cycles at 60 °C, the oxidation/reduction peaks in the d*Q*/d*V* curves become wider and less intense, indicating the deteriorating reversibility of lithiation. In contrast, the d*Q*/d*V* curve of the NCA/LIC/$Cl_{1.5}$/Li-In battery shows a larger peak area in the first cycle and a higher initial specific capacity. After 100 cycles, the shift of the oxidation/reduction peaks is small, indicating good reversibility of lithium ions after long-term charge/discharge cycling. This result is consistent with the good cycle performance shown in Fig. 2e.

Multiple characterization methods have been combined to perform on the cycled electrode mixtures of the NCA/$Cl_{1.5}$/Li-In and NCA/LIC/$Cl_{1.5}$/Li-In batteries at different operating temperatures to reveal the working mechanism. Firstly, the phase and valence states changes of the cathode layer were investigated before and after cycling with XPS. As illustrated in Fig. 3a, two distinct components can be seen in the S 2p and P 2p signals of the pristine NCA@$Li_{5.5}PS_{4.5}Cl_{1.5}$ that are split by the spin-orbit coupling effect. After cycling, the cycled cathode undergoes chemcial reactions, resulting in the oxidized species such as SO_4^{2-}, SO_3^{2-}, bridging S, PO_4^{3-} and P_2S_5 derived from the $Li_{5.5}PS_{4.5}Cl_{1.5}$ in the mixture. The emergence of these compounds leads to the formation of a high-resistance interfacial layer, which hinders Li^+-ion diffusion. In the S 2p spectra, the red peak at 161.7 eV is indicative of S atoms in the PS_4^{3-}, while the orange peak at a higher binding energy of 163.5 eV corresponding to the bridging S [41]. Two other weak peaks at 166.5 eV and 168.8 eV are also detected, belong to the SO_3^{2-} and SO_4^{2-}, respectively. For the P 2p spectra, the signature of argyrodite remains unaltered. Moreover, two additional P 2p peaks appeared at 132.6 eV and 134.0 eV are also observed in the cycled electrode [42,43]. These two peaks are assigned to the P atom in P_2S_5 and phosphate oxide due to the decomposition of $Li_{5.5}PS_{4.5}Cl_{1.5}$ electrolytes during cycling. Compared with these signals belonging to different elements for the cycled cathode at room temperature, the relative intensities of different XPS peaks significantly increase for the cathode mixture cycled under 60 °C, suggesting that the side reactions are enhanced at elevated temperatures (Fig. 3a). For the bare NCA cycled with $Li_{5.5}PS_{4.5}Cl_{1.5}$ at room temperature, strong XPS peak assigned to the PS_4^{3-} structure is observed in the P 2p spectra, suggesting a high proportion of this PS_4^{3-} in the mixture. In contrast, very weak XPS peak belonging to the PS_4^{3-} structure in the cycled bare NCA with sulfide under 60 °C. Moreover, huge amount of XPS singals of the side reaction products are detected under this elevated temperature, which also implies more intense side reaction. Based on these XPS analysis results, the higher operating temperature promotes the occurrence of side reactions. While the Cl 2p and In 3d spectra of the pristine NCA@Li_3InCl_6, the cycled NCA@Li_3InCl_6 at room and elevated temperatures show minor changes in Fig. 3b. For the In 3d spectra, XPS peaks at 446.2 eV and 453.8 eV due to the In $3d_{5/2}$ and In $3d_{3/2}$ are observed. While for the Cl 2p spectra, these XPS peaks at 199.6 eV and 201.2 eV assigned to the Cl $2p_{3/2}$ and Cl $2p_{1/2}$ are detected in the spectra, reflecting the In-Cl and/or Li-Cl bonds in Li_3InCl_6 [44]. No other energy shifts are found both in the Cl 2p and In 3d spectra of these different mixtures, suggesting that no

side reaction species exist on the surface. These above results confirm that the Li_3InCl_6 electrolyte is stable with the bare NCA during the electrochemcial cycling processes both at room and elevated temperatures. Furthermore, *ex-situ* XRD were operated on the cathode mixture after cycling at 60 °C (Figs. 3c and d). XRD refinements were conducted on the powder XRD results of cycled mixtures. The relevant refinement lattice parameters are listed in Table S5 (Supporting information). After 100 cycles, the lattice parameter *a* of NCA in contact with $Li_{5.5}PS_{4.5}Cl_{1.5}$ directly was found to be smaller than the original NCA ($a = 2.86586$ Å), while the lattice parameter *c* of the active material after cycling ($c = 14.31850$ Å) was greater than the original value ($c = 14.18720$ Å). In addition, the Li/Ni mixing degree also increased, to 2.3%. The changes in lattice constant are due to the side reaction between the exposed NCA and the unstable $Li_{5.5}PS_{4.5}Cl_{1.5}$ during cycling, which leads to the obstruction of Li^+ migration dynamics at the end of discharge, and thus the lattice structure of the NCA active material is destroyed. Several diffraction peaks were found to match well with the PDF card of Ni_xS_6, indicating that it is a byproduct. In contrast, the lattice parameters of NCA in contact with Li_3InCl_6 showed little change compared to the original NCA lattice parameters, and the Li/Ni mixing degree (only 1.5%) was also lower than that of the aforementioned active material, which ensured the stability of the NCA positive electrode structure and exhibited excellent electrochemical performance. Ultimately, SEM was applied to characterize the surface morphology of the cycled cathode and the cross-sectional morphology of the cycled samples. As shown in Fig. S4a (Supporting information), many obvious cracks and voids are observed on the surface of cathode mixture of the NCA/$Cl_{1.5}$/Li-In battery after 100 cycles when operated at 60 °C at 0.5 C. These cracks and voids are ascribed to the volume changes of the NCA active material caused by the Li-ion insertion/extraction process during cycling. While for the cycled cathode mixture of the NCA/LIC/$Cl_{1.5}$/Li-In battery, minor cracks or voids can be detected on the surface, suggesting smaller volume variations of the NCA with the Li_3InCl_6 electrolyte in the cathode. The distributions of different elements on the surface of these two kinds of cycled cathode based on the EDS mapping results also confirms the above conclusions. For the morphology of the cross-sectional section, as depicted in Fig. S5 (Supporting information), many cracks and voids are detected at the cross section of the cycled NCA/$Cl_{1.5}$, while much more dense contact are observed for the cycled NCA/LIC/$Cl_{1.5}$ interfaces. This also explains the superior electrochemcial performance of the assembled NCA/LIC/$Cl_{1.5}$/Li-In battery at 60 °C in Fig. 2e. In addition, it can be seen from EDS mapping that Cl element is enriched at the interface of NCA/$Cl_{1.5}$, indicating that the interfacial reaction products formed by bare NCA and $Li_{5.5}PS_{4.5}Cl_{1.5}$ contain Cl element, may be LiCl. It is in good agreement with the analysis of previous reports [35]. For comparison, good contact are detected for the cycled NCA/LIC/$Cl_{1.5}$ interfaces based on the SEM image and EDS mapping results (Fig. S5).

Finally, TEM was performed on the cathode mixture of NCA/LIC/$Cl_{1.5}$/Li-In battery after 100 cycles at elevated temperature to gain deeper insights into the superior battery performance. As shown in Fig. 4, the intact NCA particles are observed in the images of cycled cathode. Moreover, a uniform layer of amorphous substance with a thickness of 3 nm is detected surround the chosen NCA particle. EDX mapping results confirms that the In-containing material is homogenous distributed over the chosen particle. This phenomenon has never been observed in previous studies. During the very beginning of the cycling test at elevated temperature, Li_3InCl_6 electrolytes in the cathode mixture immediately react with the bare NCA cathode to creat an In-containing amorphous substance, which can stabilize the interface between the NCA and Li_3InCl_6 in the following electrochemcial progress, resultsing in effective Li-ion transport across the interface and delivering superior cyclability with high discharge capacities. Similarly, TEM was also conducted on the cycled cathode mixture of NCA/$Cl_{1.5}$/Li-In cell at 60 °C. EDX mapping results in Fig. S6 (Supporting information) show that Al element is detected in the $Li_{5.5}PS_{4.5}Cl_{1.5}$ electrolyte side. In other words, the Al element in NCA particles is diffused, which is associated with the side reaction between these two materials. The discharge capacities degrades rapidly due to the intense side raction at higher temperature during the cycle, as the battery performance shown in Fig. 2e.

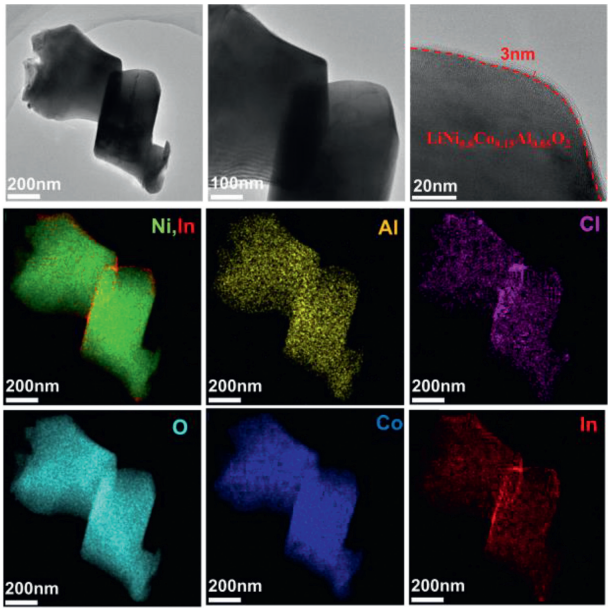

Fig. 4. TEM images and EXD mapping of the cycled cathode mixture for the assembled NCA/LIC/$Cl_{1.5}$/Li-In solid-state lithium batteries at 0.5 C at 60 °C.

In summary, a new dual-electrolyte strategy was proposed to enhance the electrochemical performances of ASSLB using the NCA cathode and $Li_{5.5}PS_{4.5}Cl_{1.5}$ electrolyte in this work. The Li_3InCl_6 electrolyte act both as an ion additive facilitated Li-ion transport over the interface and as a buffer layer to prevent spontaneous reactions and electrochemical decomposition of the $Li_{5.5}PS_{4.5}Cl_{1.5}$ during cycling, ultimately enhancing the interfacial stability. Moreover, the introduction of Li_3InCl_6 electrolyte also can mitigate the space charge effect on the assembled battery, leading to improved electrochemical performances. As expected, the NCA/LIC/$Cl_{1.5}$/Li-In battery exhibits high initial discharge performance of 237.04 mAh/g and 216.07 mAh/g at 0.1 C and 0.5 C when cycled at 60 °C, respectively. Moreover, it displays outstanding cycling performance, with a capacity retention rate of 95.92% after 100 cycles at 0.5 C at 60 °C. These findings demonstrate that the proposed dual-electrolyte layer strategy effectively enhances electrochemcial performance of NCA-based sulfide electrolyte solid-state batteries.

Declaration of competing interest

The authors declare that they have no conflict of interest.

Acknowledgments

This work was supported by the National Key Research and Development Program (No. 2021YFB2500200), the National Natural Science Foundation of China (No. 52177214). This work is also supported by China Fujian Energy Devices Science and Technology Innovation Laboratory Open Fund (No. 21C-OP202211).

References

[1] X. Yao, B. Huang, J. Yin, et al., Chin. Phys. B 25 (2016) 018802.
[2] X.B. Cheng, R. Zhang, C.Z. Zhao, et al., Chem. Rev. 117 (2017) 10403–10473.
[3] J.M. Tarascon, M. Armand, Nature 414 (2001) 359–367.
[4] J.B. Goodenough, Y. Kim, Chem. Mater. 22 (2009) 587–603.
[5] C. Wang, J. Liang, S. Hwang, et al., Nano Energy 72 (2020) 104686.
[6] S. Kim, H. Oguchi, N. Toyama, et al., Nat. Commun. 10 (2019) 1081.
[7] S. Chen, C. Yu, C. Wei, et al., Chin. Chem. Lett. 34 (2022) 107544.
[8] C. Wei, X. Liu, C. Yu, et al., Chin. Chem. Lett. 34 (2023) 107859.
[9] Q. Guo, F. Xu, L. Shen, et al., Energy Mater. Adv. 2022 (2022) 8.
[10] C. Yu, S. Ganapathy, E.R.H. van Eck, et al., J. Energy Chem. 38 (2019) 1–7.
[11] C. Liao, C. Yu, S. Chen, et al., Renewables (2023) 1–11.
[12] C. Liao, C. Yu, X. Miao, et al., Materialia 26 (2022) 101603.
[13] C. Yu, Y. Li, M. Willans, et al., Nano Energy 69 (2020) 104396.
[14] C. Yu, Y. Li, W. Li, et al., Energy Storage Mater 30 (2020) 238–249.
[15] N. Ahmad, S. Sun, P. Yu, et al., Adv. Funct. Mater. 32 (2022) 2201528.
[16] M. Yang, L. Chen, H. Li, et al., Energy Mater. Adv. 2022 (2022) 41.
[17] J.S. Kim, S. Jung, H. Kwak, et al., Energy Storage Mater 55 (2023) 193–204.
[18] X. Li, M. Liang, J. Sheng, et al., Energy Storage Mater 18 (2019) 100–106.
[19] C. Wei, C. Yu, S. Chen, et al., Electrochim. Acta 438 (2023) 141545.
[20] S. Payandeh, F. Strauss, A. Mazilkin, et al., Nano Res. Energy 1 (2022) e9120016.
[21] H. Kitaura, A. Hayashi, K. Tadanaga, et al., Electrochim. Acta 55 (2010) 8821–8828.
[22] N. Ohta, K. Takada, L. Zhang, et al., Adv. Mater. 18 (2006) 2226–2229.
[23] S. Ito, S. Fujiki, T. Yamada, et al., J. Power Sources 248 (2014) 943–950.
[24] J. Lee, Y.J. Park, J. Electrochem. Sci. Technol. 9 (2018) 176–183.
[25] A. Sakuda, H. Kitaura, A. Hayashi, et al., J. Power Sources 189 (2009) 527–530.
[26] A. Sakuda, A. Hayashi, M. Tatsumisago, Chem. Mater. 22 (2009) 949–956.
[27] C. Wei, S. Chen, C. Yu, et al., Appl. Mater. Today 31 (2023) 101770.
[28] C. Yu, F. Zhao, J. Luo, et al., Nano Energy 83 (2021) 105858.
[29] S. Chen, C. Yu, C. Wei, et al., Energy Mater. Adv. 4 (2023) 0019.
[30] C. Yu, S. Ganapathy, E. Eck, et al., Nat. Commun. 8 (2017) 1086.
[31] G. Peng, X. Yao, H. Wan, et al., J. Power Sources 307 (2016) 724–730.
[32] T.J. Park, J.B. Lim, J.T. Son, Bull. Korean Chem. Soc. 35 (2014) 357–364.
[33] W. Li, J.N. Reimers, J.R. Dahn, Solid State Ionics 67 (1993) 123–130.
[34] C.H. Lu, B.J. Shen, J. Alloys Compd. 497 (2010) 159–165.
[35] A. Banerjee, H. Tang, X. Wang, et al., ACS Appl. Mater. Interfaces 11 (2019) 43138–43145.
[36] D. Shin, J.S. Nam, C.T. Linh Nguyen, et al., J. Mater. Chem. A 10 (2022) 23222–23231.
[37] T. Tsujimura, S. Ito, K. Yoshida, et al., Solid State Ionics 383 (2022) 115970.
[38] J. Yin, X. Yao, G. Peng, et al., Solid State Ionics 274 (2015) 8–11.
[39] S.H. Jung, U.H. Kim, J.H. Kim, et al., Adv. Energy Mater. 10 (2019) 1903360.
[40] Y. Wang, Z. Wang, D. Wu, et al., eScience 2 (2022) 537–545.
[41] J. Auvergniot, A. Cassel, D. Foix, et al., Solid State Ionics 300 (2017) 78–85.
[42] J. Auvergniot, A. Cassel, J.B. Ledeuil, et al., Chem. Mater. 29 (2017) 3883–3890.
[43] C. Wei, C. Yu, R. Wang, et al., J. Power Sources 559 (2023) 232659.
[44] C. Wang, J. Liang, M. Jiang, et al., Nano Energy 76 (2020) 105015.